ACS APPLIED ENERGY MATERIALS
Cite This: ACS Appl. Energy Mater. 2018, 1, 211−219
Article
www.acsaem.org

Active Site Formation for Oxygen Reduction Reaction on Carbon-Support-Free Titanium Oxynitride with Boosted Activity in Acidic Media

Mitsuharu Chisaka,*[,†] Yusuke Yamamoto,[‡] Noriaki Itagaki,[‡] and Yuhei Hattori[‡]

[†]Department of Sustainable Energy, Hirosaki University, 3 Bunkyo-cho, Hirosaki, Aomori 036-8561, Japan
[‡]Department of Electronics and Information Technology, Hirosaki University, 3 Bunkyo-cho, Hirosaki, Aomori 036-8561, Japan

Supporting Information

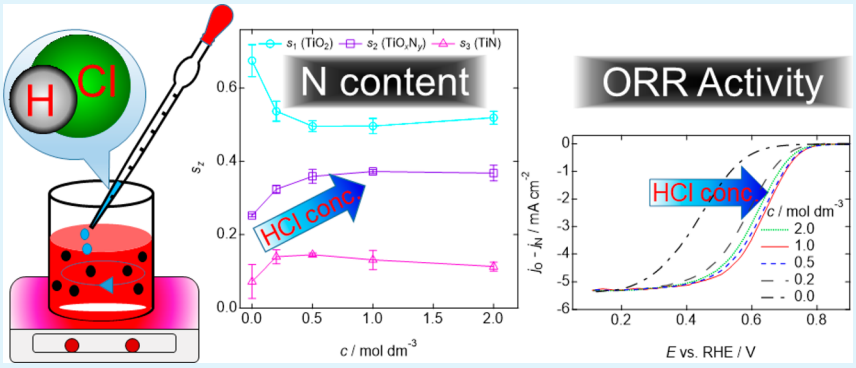

ABSTRACT: An active site formation process for recently reported carbon-support-free titanium oxynitride (TiO_xN_y) catalysts is investigated to reveal the critical factors for enhancing the oxygen reduction reaction (ORR) activity in acidic media. Neither the titanium source nor the presence of a conductive oxide support is a key to displaying activity whereas an oxidized TiN surface is revealed to be necessary. The ORR activity is successfully enhanced without using a carbon support to the level of the best carbon-supported oxide-based catalyst, zirconium oxynitride on multiwalled carbon nanotube in 0.1 mol dm^{-3} H_2SO_4 solution, mainly by optimizing hydrochloric acid concentration in the precursor dispersion to increase the surface nitrogen content. The catalyst is stable; i.e., the activity remained unchanged after 20 000 potential cycles between 0.6 and 1.0 V versus reversible hydrogen electrode.

KEYWORDS: *polymer electrolyte fuel cell, proton exchange membrane fuel cell, cathode, nonplatinum, titania*

1. INTRODUCTION

Energy storage and conversion devices have attracted increasing interest for reducing emissions from vehicles by replacing conventional combustion engines with electric motors. Lithium ion batteries, which have already been commercialized successfully in portable electronic devices and hybrid vehicles, need a long charging time and large mass by themselves when they are used in electric vehicles without a gasoline engine. The system cost and performance advancement of lithium ion batteries, so-called post lithium ion batteries, i.e., lithium−air/lithium−sulfur batteries and polymer electrolyte fuel cells (PEFCs), have been of interest and recently analyzed by several groups. It was reported that PEFCs are suitable to drive vehicles, which operate over distances greater than 300 miles or carry high loads, such as buses and tracks.[1,2] Several minutes of refueling time also make this energy conversion technology promising; however, the current usage of platinum in a 114 kW PEFC stack for a generic sedan is estimated to be in the range 22−38 g,[2] which is unacceptably high considering the depleting world reserve of platinum group metals (PGMs), i.e., 67 000 tons.[3] Platinum-based nanoparticles on carbon supports have been used in the anode and the cathode of PEFCs to catalyze hydrogen oxidation reaction (HOR) and oxygen reduction reaction (ORR), respectively. Since ORR is 5 orders of magnitude slower than HOR on platinum metal,[4] significant efforts have been made to reduce the Pt loading of the cathode. The ORR activity enhancement by optimizing the composition of platinum−cobalt catalysts and improvement of platinum utilization by employing solid-core-type carbon supports has been performed in the vehicle industry; however, further reduction of platinum loading is still needed.[5]

Development of nonplatinum catalysts, particularly those free from PGM, is another option to solve the above-mentioned issue. Over the past decade, only two types of non-PGM catalysts have been reported for use in automotive PEFC

Received: November 3, 2017
Accepted: December 26, 2017
Published: December 26, 2017

DOI: 10.1021/acsaem.7b00100
ACS Appl. Energy Mater. 2018, 1, 211−219

cathodes due to the severely corrosive environment: high operating potential of 0.6−1.0 V versus reversible hydrogen electrode (RHE)[6] and strong acidity (pH < 1).[7] The most widely developed non-PGM catalyst type is the so-called Fe(Co)/N/C catalyst, and the greatest volume is graphitic carbons with a high density of defects.[7−14] Another catalyst type is the oxide-based one, containing group IV or V metals.[15−30] The advantage of this catalyst type is chemical stability, which prevents leaching in acidic media,[15−18] whereas the disadvantage is poor conductivity that makes activity evaluation difficult.[19] To display the activity of oxide-based catalysts, various conductive carbon supports like carbon black,[20−23] carbon nanotubes,[24−26] activated carbon fiber,[27] and reduced graphene oxide sheets[28−30] have been utilized. Therefore, in both of these non-PGM catalyst types, corrosion of carbon supports should be prevented, which is accelerated during the startup/shutdown of the cell when the cathode voltage is increased up to ∼1.4 V by a reverse-current decay mechanism.[31] Besides, recent studies for these two catalyst types indicate that performances of single cells, employing a non-PGM catalyst-cathode, decreased even if they were operated below 1 V.[14,26] Dodelet et al., the pioneers of the Fe/N/C catalyst, recently reported that slow oxidation of carbon supports was the main cause of rapid performance decay when the cell voltage was maintained at 0.6 V.[14] This is because carbon oxidation (eq 1) occurs above 0.207 V versus standard hydrogen electrode and the number of reaction sites for eq 1 on the Fe/N/C catalyst should be higher than that of carbon black in the commercial carbon-supported platinum (Pt−C) catalyst, owing to the defective nature of carbons in Fe/N/C.

$$C + 2H_2O \rightarrow CO_2 + 4H^+ + 4e^- \quad (1)$$

We recently reported stability test results of multiwalled carbon-nanotube-supported zirconium oxynitride (ZrO_xN_y-MWCNT), which was synthesized via decomposition of zirconium oxyphthalocyanine (ZrOPc), in a single cell.[26] The cell was operated at a constant current density of 0.1 A cm^{-2} for 2 weeks, and the cell voltage declined sharply during the first 100 h at a degradation rate of 2 mV h^{-1}. Although the source of degradation for ZrO_xN_y-MWCNT is still unclear, corrosion of carbons that originated from ZrOPc and MWCNTs should not be negligible as they were pyrolyzed under NH_3 gas to create defects.[26]

Although significant efforts have been made to develop highly active non-PGM catalysts, the stability is still lower than that of commercial Pt−C catalyst, even when operated under 1 V in acidic PEFC cathodes. Removal of carbon supports from non-PGM catalysts is quite challenging, but is a promising route to increase stability, as confirmed for PGM-based catalysts.[32−35] We recently synthesized a carbon-support-free titanium oxynitride (TiO_xN_y) via a solution-phase combustion route, in which Ti_4O_7 fibers (as support), TiF_4, and urea were stirred in HCl solution with heating, followed by pyrolysis under N_2.[36] The resulting TiO_xN_y catalysts exhibited a limiting current plateau similar to that of commercial Pt−C catalysts in a half cell employing 0.1 mol dm^{-3} H_2SO_4 solution. Several experiments revealed that trace carbon from the urea precursor was not a source of the activity, which was the highest among reported carbon-support-free oxide-based catalysts; however, the half-wave potential was 0.63 V versus RHE which is still lower compared with those of state-of-the-art Fe/N/C catalysts[10−14] and ZrO_xN_y-MWCNT,[26] which are the best among ever reported carbon-supported oxide-based catalysts. In addition, the Ti_4O_7 phase of the support disappeared during N_2-pyrolysis with urea to form a mixture of rutile TiO_2 and TiN. Although the top surface was revealed to be N-doped amorphous TiO_2, the source remained unclear because two Ti-containing starting materials, Ti_4O_7 and TiF_4, were used.[36] The formation mechanism of the active sites on this complex carbon-support-free catalyst should be clarified for further enhancement of activity of this catalyst type.

In this study, the critical factors for enhancing the ORR activity of TiO_xN_y catalysts were determined. Unexpectedly, the concentration of HCl solution used as the dispersant of starting materials was found to control the surface composition, and by increasing it above 0.5 mol dm^{-3}, the activity was successfully enhanced from the previous work to be almost the same as that of ZrO_xN_y-MWCNT.

2. EXPERIMENTAL SECTION

2.1. Synthesis of the Catalysts. The TiO_xN_y catalysts were synthesized using the solution-phase combustion route[36] with the following three modifications: support-free, use of various titanium sources and various HCl concentration in the precursor dispersion, *c*, values. First, TiF_4 powder (Sigma-Aldrich Co., St. Louis, MO) or titanium oxysulfate powder ($TiOSO_4$, Kishida Chemical Co. Ltd., Osaka, Osaka, Japan) and urea powder ($(NH_2)_2CO$, Wako Chemical Industries Ltd., Osaka, Osaka, Japan) were mixed in a certain amount of distilled water by magnetically stirring with a polytetrafluoroethylene (PTFE) bar at room temperature. The beaker used for the mixing was made of PTFE and the outside bottom was coated with a PTFE−carbon composite to assist heating on a hot stirrer. The mass ratio of urea to TiF_4- or $TiOSO_4$-derived TiO_2, *u*, was set at 100, unless otherwise noted. Next, 35% (w/w) HCl solution (Kishida Chemical Co. Ltd., Osaka, Osaka, Japan) was added to the solution with continuous stirring. The *c* was varied in the range 0−2 mol dm^{-3}, and the volume of the solution was maintained at 406−407 cm^3 at any *c*. Then, the PTFE beaker was placed on another stirrer preheated to 523 K, stirred continuously until the solvent evaporated, and then dried in a convection oven overnight at 380 K. The dried powders were ground using an agate mortar. Subsequently, each precursor powder was placed in an alumina boat which was then placed in a horizontal quartz-tube furnace. The tube was slowly evacuated and purged with N_2 gas, and the powder samples were heated from room temperature to various temperatures at a rate of 10 K min^{-1}. The temperature was maintained for 2 h unless otherwise noted. The samples were then cooled to room temperature at an uncontrolled rate. The N_2 flow rate was 100 sccm during pyrolysis. After pyrolysis, the powders were ground in an agate mortar. It is noted that some solid byproducts became attached to the inner wall of the quartz tube during pyrolysis. The solid byproducts can stop the gas flow if they block the narrow opening of the quartz tube, which can be extremely dangerous. We used a quartz tube more than three times longer than the heating zone, such that there is sufficient space for byproduct accumulation inside the tube to avoid blockage. After pyrolysis and ejection of the alumina boats, the byproducts were easily removed by washing the tube with water. The TiO_xN_y catalyst that exhibited the highest activity was further pyrolyzed under NH_3 gas. They were placed in an alumina boat and then placed in another horizontal quartz-tube furnace and were heated from room temperature to 873 K at a rate of 10 K min^{-1}; the temperature was maintained for various durations. The flowing gases at and under 873 K were NH_3 and N_2, respectively, and the flow rate of both gases was 100 sccm.

2.2. Characterization. The morphology of the TiO_xN_y catalysts was investigated using a transmission electron microscope (JEM-2100, JEOL, Akishima, Tokyo, Japan). The bulk crystal structures of catalysts were analyzed using an X-ray diffractometer (MiniFlex 600, Rigaku Co., Akishima, Tokyo, Japan) with Cu Kα radiation generated at 40 kV and 15 mA (scan rage = 20−80°, step size = 0.02°, and scan

DOI: 10.1021/acsaem.7b00100
ACS Appl. Energy Mater. 2018, 1, 211−219

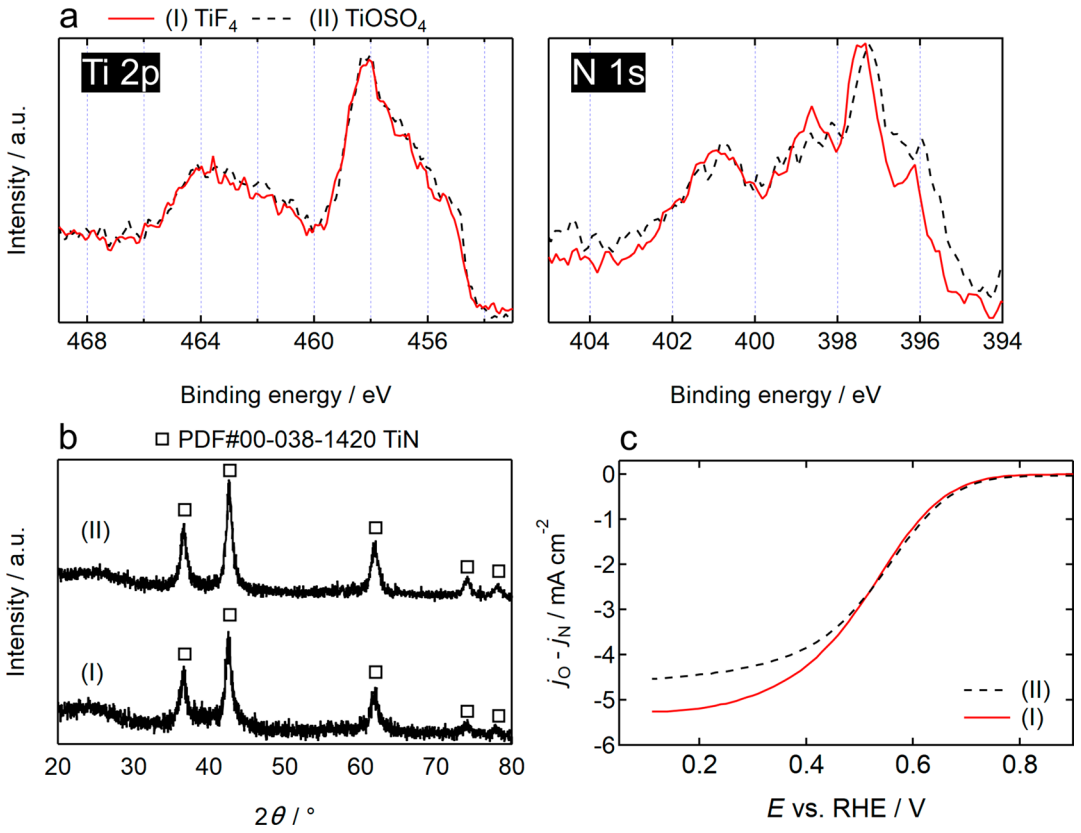

Figure 1. (a) XP Ti 2p and N 1s spectra, (b) XRD patterns, and (c) RDE voltammograms of TiO_xN_y catalysts synthesized by mixing urea and one of two different titanium precursors: (I) TiF_4 and (II) $TiOSO_4$ in 0.2 mol dm^{-3} HCl solution followed by pyrolysis at 1123 K. The scans were performed under N_2 and O_2 atmospheres, with a rotation speed of 1500 rpm and a scan rate of −5 mV s^{-1} (cathodic) in 0.1 mol dm^{-3} H_2SO_4. The catalyst loading, m, was 1.0 mg cm^{-2}.

rate = 2° min^{-1}). The crystallite size of some catalysts, D, was estimated by fitting the peaks with Scherrer's equation

$$D = 0.94\lambda/\beta \cos\theta$$

where λ is the wavelength of the X-ray and β is the full width at half-maximum.

The surface crystal structures were evaluated using a Raman spectrometer (NRS-5100, JASCO Co. Ltd., Hachioji, Tokyo, Japan) with a 532 nm laser. The chemical states of the catalysts were determined using an X-ray photoelectron spectrometer (PHI 5000 VersaProbe, ULVAC-PHI, Inc., Chigasaki, Kanagawa, Japan) with an Al Kα X-ray source (1486.6 eV). The peak shifts due to surface charge were corrected using the binding energy of C 1s (284.8 eV), which originated from the hydrocarbon contaminants from the spectrometer. As the contributions from the hydrocarbon and TiO_xN_y to O 1s spectra cannot be distinguished from each other, only Ti 2p and N 1s spectra were used for the analyses. The spectra were acquired at three different points of each sample mounted on a holder. Then for some catalysts, Ti 2p and N 1s spectra were analyzed by fitting with six and four symmetric peaks, respectively, after subtracting Shirley-type background, and then the average area fraction of each peak was calculated.

2.3. ORR Activity and Selectivity Measurements. Rotating disk electrode (RDE) and rotating ring−disk electrode (RRDE) voltammograms were obtained to evaluate the ORR activity and selectivity, respectively, of the catalysts. The catalyst, 5% w/w Nafion ionomer solution (510211, Sigma-Aldrich Co., St. Louis, MO), and isopropyl alcohol were sonicated together for 1200 s and then further mixed using a planetary mixer (MAZERUSTAR KK-250S, Kurabo Co., Osaka, Osaka, Japan) for 180 s to obtain a homogeneous catalyst ink. The mass fraction of Nafion in the catalyst layer for TiF_4- and $TiOSO_4$-derived TiO_xN_y were set at 0.05 and 0.20, respectively. Before coating the catalyst layer, a glassy carbon (GC) disk (4 mm diameter)−platinum ring (5 mm inner diameter and 7 mm outer diameter) electrode (012613, BAS Co., Sumida-ku, Tokyo, Japan) was polished with 1.0 and 0.05 μm alumina slurries, washed with distilled water and ethanol. Then, the electrodes were dried in air at 320 K using a convection oven for at least 600 s. The catalyst loading, m, was varied between 0.6 and 2.0 mg cm^{-2} by controlling the amount of the catalyst ink dropped onto the GC electrode. Catalysts currently in use require a large m value to form a uniform coating on the GC surface, owing to the high density because they are free of carbon supports. A conventional three-electrode cell was used for the electrochemical measurements performed in 0.1 mol dm^{-3} H_2SO_4 at room temperature. The catalyst-coated GC disk−Pt ring electrode, a carbon rod (diameter: 5 mm, C-072591, Nilaco Co., Chuo-ku, Tokyo, Japan), and Ag/AgCl (3 M NaCl) electrode (RE-1B, BAS Co., Sumida-ku, Tokyo, Japan) were used as the working, counter, and reference electrodes, respectively. The working electrode was set on a rotator (RRDE-3 or RRDE-3A, BAS Co., Sumida-ku, Tokyo, Japan). All working electrode potentials were referenced to the RHE. After sequentially bubbling O_2 and N_2 for 1800 s, the RDE and RRDE voltammograms were recorded by applying a disk potential (E) from 1.26 to 0.11 V (cathodic) at a scan rate of 5 mV s^{-1} and a rotation speed of 1500 rpm, using a bipotentiostat (model 2323 or 704B, BAS Co., Sumida-ku, Tokyo, Japan). The ring potential was maintained at 1.26 V to obtain the RRDE voltammograms. The ORR was measured by background-corrected current density, $j = j_O - j_N$, the difference between the current per unit geometrical area, S, of the GC disk electrode obtained in O_2 ($j_O = I_O\ S^{-1}$) and in N_2 ($j_N = I_N\ S^{-1}$). The values of hydrogen peroxide yield, $\chi_{H_2O_2}$, and number of electrons transferred per oxygen molecule, n, were calculated by analyzing the RRDE voltammograms according to the following equations:

DOI: 10.1021/acsaem.7b00100
ACS Appl. Energy Mater. 2018, 1, 211−219

$$\chi_{H_2O_2}(\%) = 100\frac{2I_r/N}{-I_d + I_r/N}$$

$$n = -4I_d/(-I_d + I_r/N)$$

where I_d and I_r denote the disk and ring currents, respectively, after the background correction described above, and N is the collection efficiency (0.424) provided by the manufacturer (BAS Co.). As a reference, Pt−C catalyst (36.7% w/w Pt on Ketjen Black, TEC10E40E, Tanaka Kikinzoku Kogyo K.K, Chiyoda-ku, Tokyo, Japan) was used under identical conditions, except for the scan direction and electrolyte, from 0.11 to 1.26 V (anodic), and 0.1 mol dm^{-3} $HClO_4$ solution, respectively, because (bi)sulfate adsorption on platinum catalysts is known to block the initial adsorption of O_2 to decrease the activity.[37]

3. RESULTS AND DISCUSSION

3.1. Effect of Titanium Source. In a previous study, in which Ti_4O_7 fiber was used as the support, X-ray diffraction (XRD) analysis showed that rutile TiO_2 and TiN were formed in bulk after pyrolyzing the mixture of Ti_4O_7 support, TiF_4, and urea.[36] Although ultraviolet Raman spectroscopy and X-ray photoelectron spectroscopy (XPS) analyses showed that the ORR-active top surface was N-doped amorphous TiO_2, the critical factors for the emergence of the ORR activity were unclear because the amorphous TiO_xN_y species could originate from both Ti_4O_7 and TiF_4. In this study, support-free TiO_xN_y catalysts were synthesized to clarify the key factors for displaying activity on this complex catalyst. First, two catalysts were synthesized from different precursors, TiF_4 and $TiOSO_4$, under identical conditions.

Figure 1 shows the XP Ti 2p and N 1s spectra, XRD patterns, and RDE voltammograms of the two catalysts. Both catalysts displayed almost the same spectra and a single TiN phase, as shown in Figure 1a,b, respectively. Besides, j values were almost the same as those at potential $E \geq 0.5$ V (Figure 1c). These results clearly indicate that the Ti source did not affect the surface chemical states, bulk crystal structure, or the resulting activity. Neither F atoms from TiF_4 nor S atoms from $TiOSO_4$ remained at the catalyst surface (Figure S1, Supporting Information), implying that these atoms from the precursors do not contribute to the activity. When Ti_4O_7 powders were solely used instead of TiF_4 or $TiOSO_4$, the crystal structure was converted to a single rutile TiO_2 phase with no activity (Figure S2, Supporting Information). In a previous paper, N_2-pyrolysis of the mixture of three components, TiF_4, Ti_4O_7, and urea, resulted in the mixed phase of rutile TiO_2 and TiN with clear activity.[36] These results indicate that the active site of the previous catalyst was located on the oxidized surface of TiN and the source was TiF_4, not Ti_4O_7. For the preparation of TiO_xN_y catalysts using the present solution-phase combustion route, it was found that at least a nonoxide titanium precursor is necessary to produce ORR-active sites on a conductive TiN surface and moisture-sensitive TiF_4 can be replaced by stable $TiOSO_4$ without decrease in activity.

3.2. Effect of Hydrochloric Acid Concentration in the Precursor Dispersion. HCl has been used as a dispersant in the solution-phase combustion synthesis of TiO_xN_y nanoparticles to lower the pH of the dispersion to below 1 for complete hydrolysis of the precursor TiF_4 and generate titanium hydroxides.[38,39] We show here for the first time another effect of hydrochloric acid. Figure 2a shows the XRD patterns of TiO_xN_y catalysts for five different c values.

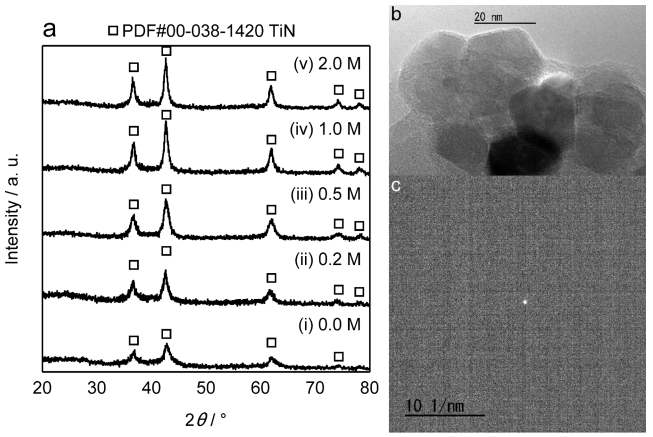

Figure 2. (a) XRD patterns of TiF_4-derived TiO_xN_y catalysts for five different c values: (i) 0.0, (ii) 0.2, (iii) 0.5, (iv) 1.0, and (v) 2.0 mol dm^{-3}. The pyrolysis temperature was 1123 K. (b) TEM image and (c) SAED pattern of the TiF_4-derived TiO_xN_y catalyst synthesized at c = 1.0 mol dm^{-3} after pyrolysis at 1123 K.

Although the pyrolysis temperature was set at 1123 K, the peaks assigned to a single TiN phase became sharper with increasing c and the resulting D values calculated from Scherrer's equation are 7.1, 7.3, 7.3, 11.1, and 11.6 nm when c was 0, 0.2, 0.5, 1, and 2 mol dm^{-3} respectively. In general, D increases with increasing the pyrolysis temperature or duration. However, all the catalysts shown in Figure 2a were synthesized under identical pyrolysis conditions of 1123 K and 2 h. The precise mechanism for the formation of TiN is not clear at this stage; however, the synthesis processes of TiN[40] and nitrogen-doped TiO_2[41] have been reported to be exothermic. The amount of nitrogen source formed via reaction of decomposed urea and HCl, which is discussed later in 3.3, should increase with increasing c. The results shown in Figure 2a suggest that some exothermic reactions proceeded to increase the local temperature, i.e., the temperature of the catalyst surface and thus to increase D at higher c. The Raman spectra indicate that the TiN surface was oxidized to amorphous TiO_2 and clear rutile peaks appeared when c was increased to 2.0 mol dm^{-3} (Figure S3, Supporting Information). The amorphous nature of the surface of the 1.0 mol dm^{-3} sample was also confirmed by the transmission electron microscopy (TEM) image and the selected area electron diffraction (SAED) pattern as shown in Figure 2b,c, respectively.

The c value also significantly affected the surface composition and chemical states, as shown in Figure 3. The Ti 2p level splits into Ti $2p_{3/2}$ and $2p_{1/2}$ sublevels by spin−orbit coupling, displaying doublets in the spectra. All five catalysts showed three pairs of doublets, whereas the area ratio strongly depended on c. The Ti $2p_{3/2}$ peak at 458.1−458.3 eV, assigned to Ti^{4+} in amorphous TiO_2,[36,42] occupied the largest area in any spectrum. However, the percentage of the TiO_2 phase in the Ti 2p spectrum decreased with increasing c due to the growth of two shoulders: the larger one at 456−457 eV is assigned to one or more bonding states in TiO_xN_y,[42,43] and the smaller one at 455 eV is assigned to N−Ti−N bonding in TiN.[42−44] The area fractions of these three components are summarized in Figure 4. The area fraction of the TiO_2 phase, s_1, decreased whereas that of the TiO_xN_y phase, s_2, increased with increasing c up to 0.5 mol dm^{-3}, indicating that the surface nitrogen content of TiO_xN_y was increased by adding HCl into the precursor dispersion. At any c value, the surface

DOI: 10.1021/acsaem.7b00100
ACS Appl. Energy Mater. 2018, 1, 211−219

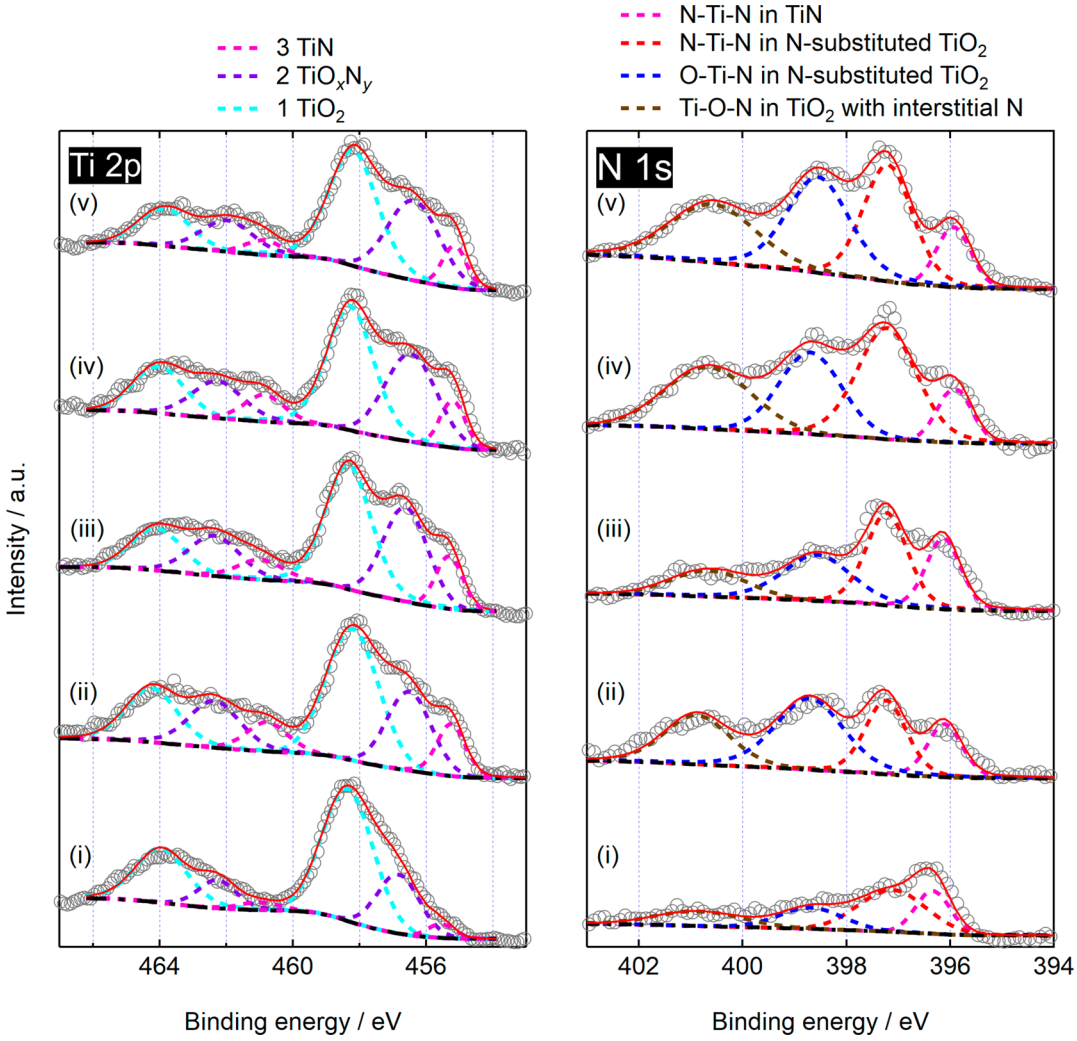

Figure 3. XP Ti 2p and N 1s spectra of TiF_4-derived TiO_xN_y catalysts for five different c values: (i) 0.0, (ii) 0.2, (iii) 0.5, (iv) 1.0, and (v) 2.0 mol dm^{-3}. All the spectra (○) are shown with overall fitting (—) and deconvolution into several peaks (---) after subtracting Shirley-type background (···). The pyrolysis temperature was 1123 K.

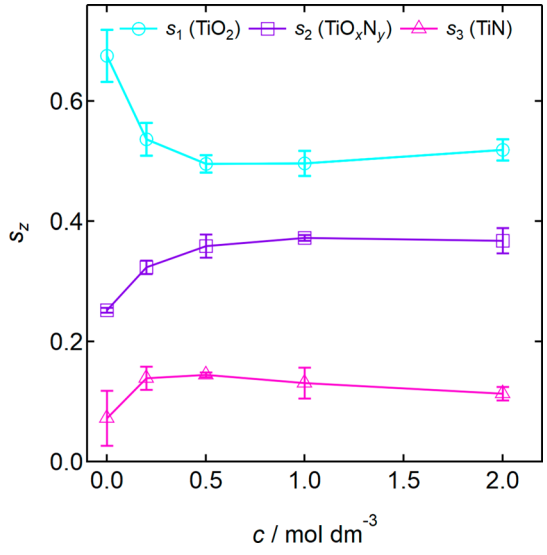

Figure 4. Area fractions of the three components in Ti 2p region versus c, calculated from Figure 3.

TiN content, s_3, was low and was maintained below 0.15, lower than the detection limit of the Raman spectrometer. The chemical states of the doped nitrogen atoms were investigated using the N 1s spectra (right-hand side of Figure 3). At the lowest c of 0.0 mol dm^{-3}, the N 1s spectrum was very noisy, indicating that the amount of doped nitrogen atoms was small, as predicted from the corresponding Ti 2p spectrum. However, the spectrum became progressively less noisy with increasing c, mainly due to the growth of two central peaks at ~397 and ~399 eV, which are assigned to N−Ti−N and O−Ti−N bonding, respectively, both in the N-substituted TiO_2 lattice.[45,46] Thus, the increased surface nitrogen content at high c was from TiO_xN_y which is in good agreement with the results from the Ti 2p spectra. It is noted that when c = 0.0 mol dm^{-3}, the amount of surface nitrogen was low whereas the area fraction of the peak at ~397 eV was the highest among the five catalysts shown in Figure 3 indicating that most of the TiN surface was oxidized to TiO_xN_y at the lowest c. As D was the lowest at c = 0.0 mol dm^{-3}, the larger area of TiN was suggested to be in contact with air moisture and thus could more easily be oxidized compared with other catalysts.

3.3. ORR Activity and Selectivity. Figure 5 shows the ORR activity of the five different catalysts with different c

DOI: 10.1021/acsaem.7b00100
ACS Appl. Energy Mater. 2018, 1, 211−219

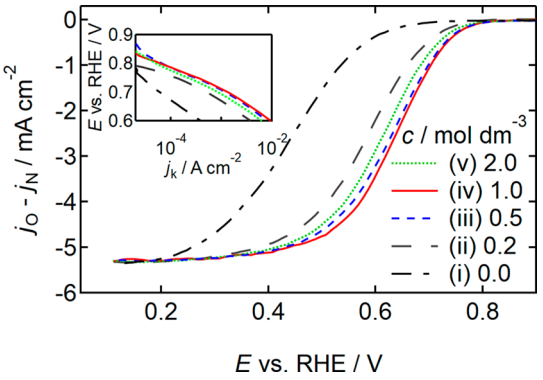

Figure 5. RDE voltammograms of TiF_4-derived TiO_xN_y catalysts for five different c values: (i) 0.0, (ii) 0.2, (iii) 0.5, (iv) 1.0, and (v) 2.0 mol dm^{-3}. The optimized pyrolysis temperatures were 1223, 1123, and 1173 K for i, ii–iv, and v, respectively. The pyrolysis duration was 2 h for i, iii–v, and 4 h for ii. The scans were performed under N_2 and O_2 atmospheres, with a rotation speed of 1500 rpm and a scan rate of −5 mV s^{-1} (cathodic) in 0.1 mol dm^{-3} H_2SO_4. The m value was 2.0 mg cm^{-2}.

values after optimizing the pyrolysis temperature for each (Figure S4–S8, Supporting Information). The mass ratio of urea to TiF_4-derived TiO_2, u, was also optimized to 100 (**Figure S9**, Supporting Information). As the density of some catalysts was so high and the surface area was small, the GC surface was visible to form so-called catalyst islands when m was low. Therefore, a high m value of 2.0 mg cm^{-2} was used for uniform coating of the GC surface. The activity of TiO_xN_y increased with increasing c up to 0.5 mol dm^{-3}; the activity was kept almost constant with further increase of c. The Tafel plots with kinetic current density, j_k,[39] are shown in the inset. The Tafel slopes were within 76–82 mV dec^{-1} at $c \geq 0.5$ mol dm^{-3}. The activity trend agrees well with the s_2 trend shown in Figure 4. Similarly, both activity and s_2 were maximized by optimizing the u value to 100 (Figure S9, Supporting Information). These results strongly suggest that the active sites were hosted in TiO_xN_y. Analysis of the N 1s spectra revealed that most N atoms in the TiO_xN_y were the ones substituted in TiO_2. We previously reported that O defects on TiO_2 formed by substitutional nitrogen doping acted as the adsorption sites for O_2 molecules, which should be the first step for ORR.[36] Thus, present results agree well with previous reports. However, why the nitrogen-doping level on TiO_2 increased with increasing c is unexplained because HCl is free from nitrogen atoms. After mixing the precursors, i.e., before the pyrolysis, the main product detected by the XRD patterns when $c > 0$ was NH_4Cl. Urea decomposed completely into ammonium ions and carbonic acid in acidic media.[47]

$$\text{urea} \rightarrow NH_4^+CNO^-$$

$$NH_4^+CNO^- + 2H^+ + 2H_2O \rightarrow 2NH_4^+ + H_2CO_3$$

The precursor dispersion used in this study is strongly acidic (pH ≤ 1 at $c \geq 0.2$ mol dm^{-3}). The NH_4Cl synthesized after

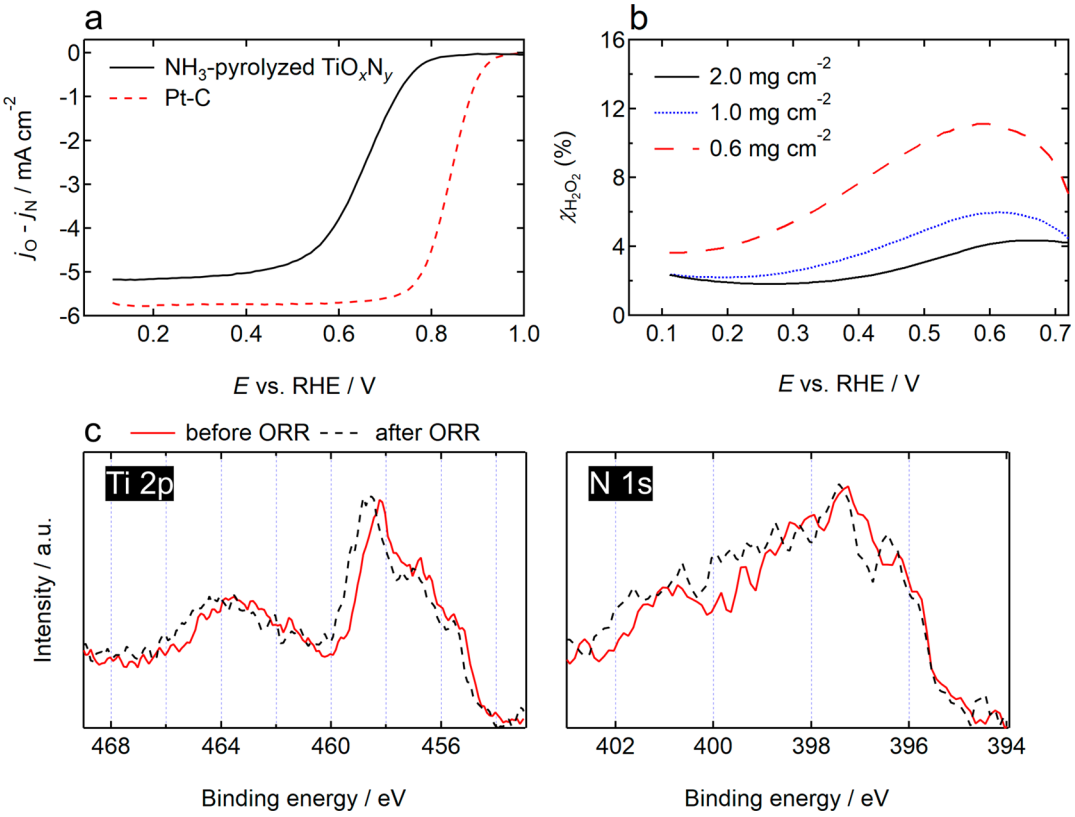

Figure 6. (a) RDE voltammograms of NH_3-pyrolyzed TiO_xN_y (m = 2.0 mg cm^{-2}) and commercial Pt–C (m = 0.2 mg cm^{-2} and corresponding Pt loading was 0.07 mg cm^{-2}) catalysts, (b) $\chi_{H_2O_2}$–E curves for TiO_xN_y with 3 different m values, and (c) XP Ti 2p and N 1s spectra of the TiO_xN_y before and after the ORR tests. The c for TiO_xN_y was 1.0 mol dm^{-3}, and pyrolyses were performed twice, the first at 1123 K for 2 h under N_2 and the second at 873 K for 1.5 h under NH_3. The scans were performed under N_2 and O_2 atmospheres, with a rotation speed of 1500 rpm and a scan rate of −5 mV s^{-1} (cathodic) in 0.1 mol dm^{-3} H_2SO_4 for TiO_xN_y and 5 mV s^{-1} (anodic) in 0.1 mol dm^{-3} $HClO_4$ for Pt–C.

DOI: 10.1021/acsaem.7b00100
ACS Appl. Energy Mater. 2018, 1, 211–219

precursor mixing should originate from the reaction between the ammonium ions released from urea and the chloride ions from HCl solvent. These XRD results indicate that the NH_4Cl acted as a nitrogen source to produce TiN with various possible routes, including the decomposition to NH_3 and HCl.[48,49] As *c* increased, the amount of NH_4Cl should increase before pyrolysis, and thus, surface nitrogen content on the oxidized TiN after pyrolysis also increased. Therefore, unexpectedly, *c* significantly boosted the activity.

The best catalyst, i.e., the 1 mol dm^{-3} sample, was further pyrolyzed under NH_3 gas, producing reactive nitrogen by decomposition at 873 K. Figure 6 compares the RDE voltammogram with that of commercial Pt−C catalysts. The TiO_xN_y activity was successfully enhanced from the previous work[36] without using carbon supports to be almost the same as the best carbon-supported oxide-based catalyst reported to date, ZrO_xN_y-MWCNT[26] (Table S1, Supporting Information). However, a large gap is still observed when compared with Pt−C in 0.1 mol dm^{-3} $HClO_4$; the difference in half-wave potential is 0.15 V. As the aggregation of the TiO_xN_y catalyst was not severe enough, the *m* value could be reduced to 0.6 mg cm^{-2} without forming catalyst islands on the GC surface. Therefore, the effect of the *m* value on reaction mechanism was investigated using RRDE voltammograms, and the results are shown in Figure 6b. The $\chi_{H_2O_2}$ value decreased with increasing *m*, indicating that some hydrogen peroxide molecules, produced near the GC electrode side ($O_2 + 2H^+ + 2e^- \rightarrow H_2O_2$), were decomposed ($H_2O_2 \rightarrow H_2O + 0.5\ O_2$) or further reduced electrochemically ($H_2O_2 + 2H^+ + 2e^- \rightarrow 2H_2O$) before passing through the thicker catalyst layers for detection at the ring electrode. However, the $\chi_{H_2O_2}$ value was lower than 11% at any *E* value, even at the lowest *m* of 0.6 mg cm^{-2}, which indicates that the ORR mostly proceeded via a 4-electron pathway involving direct reduction of oxygen molecules to water ($O_2 + 4H^+ + 4e^- \rightarrow 2H_2O$). As mentioned earlier, the highest activity among reported oxide-based catalysts is from ZrO_xN_y-MWCNT[26] (Table S1, Supporting Information). The drawback of the ZrO_xN_y-MWCNT catalyst was low ORR selectivity to 4-electron pathway with the highest $\chi_{H_2O_2}$ of 35% at $E = 0.6$ V and $m = 0.55$ mg cm^{-2} because N-doped carbon supports produced H_2O_2 at low *E*.[26] The selectivity of the present carbon-support-free TiO_xN_y catalyst is much higher than the ZrO_xN_y-MWCNT and previously reported TiO_xN_y catalysts supported on carbon black.[38,39] Stability of the chemical states on the best TiO_xN_y catalyst is investigated by obtaining XP spectra after ORR tests, and the results are compared with those obtained before ORR tests (Figure 6c). Neither Ti 2p nor N 1s spectra changed significantly during the ORR tests, indicating that the TiO_xN_y was stable under the experimental conditions. Further, the TiO_xN_y catalyst exhibited excellent durability against load cycle tests in which the potential was cycled between 0.6 and 1.0 V (Figure S10, Supporting Information). However, the durability against startup/shutdown tests needs improvements; the decrease in activity after 5000 potential cycles between 1.0 and 1.5 V is not negligible (Figure S11, Supporting Information). The degradation mechanism should be investigated for the improvements to use this catalyst without keeping the *E* below 1 V.

4. CONCLUSION

The critical factors for emergence of ORR activity on carbon-support-free TiO_xN_y catalysts were investigated. Active sites were located on oxidized TiN surface, and the HCl concentration in the precursor dispersion was found to be key for the activity emergence and enhancement of surface nitrogen content. After systematic optimizations of the HCl concentration, pyrolysis temperature, and urea content, as well as the additional NH_3-gas pyrolysis, the activity of carbon-support-free TiO_xN_y was boosted to almost the same as the best carbon-supported oxide-based catalyst. The surface chemical states were not altered by the ORR tests. The enhanced activity remained constant after 20 000 potential cycles between 0.6 and 1.0 V versus RHE, whereas it declined after 5000 cycles between 1.0 and 1.5 V which indicates the need to keep the potential below 1 V by procedures on the system level.

■ ASSOCIATED CONTENT

Supporting Information

The Supporting Information is available free of charge on the ACS Publications website at DOI: 10.1021/acsaem.7b00100.

Experimental details, XP spectra, XRD patterns, RDE voltammograms, Raman spectra, comparison of ORR activities in the literature, and durability test result (PDF)

■ AUTHOR INFORMATION

Corresponding Author

*E-mail: chisaka@hirosaki-u.ac.jp.

ORCID

Mitsuharu Chisaka: 0000-0002-9394-200X

Notes

The authors declare no competing financial interest.

■ ACKNOWLEDGMENTS

This work was partially supported by a Grant-in-Aid for Scientific Research (C), 17K06180, from the Ministry of Education, Culture, Sports, Science, and Technology (MEXT) in Japan, a research grant from the Nippon Sheet Glass Foundation for Materials Science and Engineering, a research grant, KJ-2539, from the Kato Foundation for Promotion of Science in Japan, a research grant for young scientists from Nippon Life Insurance Foundation in Japan, a research grant from the Murata Science Foundation in Japan, and a research grant from Yashima Environment Technology Foundation in Japan. The XP spectra were acquired at the University of Tokyo supported by the Nanotechnology Platform of the MEXT in Japan.

■ ABBREVIATIONS

PGM, platinum group metal
ORR, oxygen reduction reaction
ZrO_xN_y, zirconium oxynitride
PEFC, polymer electrolyte fuel cell
HOR, hydrogen oxidation reaction
RHE, reversible hydrogen electrode
Pt−C, carbon-supported platinum
TiO_xN_y, titanium oxynitride

■ REFERENCES

(1) Eberle, U.; von Helmolt, R. Sustainable Transportation Based on Electric Vehicle Concepts: a Brief Overview. *Energy Environ. Sci.* **2010**, 3, 689−699.

DOI: 10.1021/acsaem.7b00100
ACS Appl. Energy Mater. 2018, 1, 211−219

(2) Gröger, O.; Gasteiger, H. A.; Suchsland, J. P. Review—Electromobility: Batteries or Fuel Cells? *J. Electrochem. Soc.* **2015**, *162*, A2605−A2622.
(3) U.S. Department of the Interior. *Mineral Commodity Summaries*; 2017; p 126.https://minerals.usgs.gov/minerals/pubs/mcs/2017/mcs2017.pdf (Last accessed on Nov. 2, 2017).
(4) Larminie, J.; Dicks, A. In *Fuel Cell Systems Explained*, 2nd ed.; John Wiley and Sons Ltd.: Chichester, 2003; p 51.
(5) Yoshida, T.; Kojima, K. Toyota MIRAI Fuel Cell Vehicle and Progress Toward a Future Hydrogen Society. *Electrochem. Soc. Interface* **2015**, *24*, 45−49.
(6) Ohma, A.; Shinohara, K.; Iiyama, A.; Yoshida, T.; Daimaru, A. Membrane and Catalyst Performance Targets for Automotive Fuel Cells by FCCJ Membrane, Catalyst, MEA WG. *ECS Trans.* **2011**, *41*, 775−784.
(7) Jaouen, F.; Herranz, J.; Lefevre, M.; Dodelet, J. P.; Kramm, U. I.; Herrmann, I.; Bogdanoff, P.; Maruyama, J.; Nagaoka, T.; Garsuch, A.; Dahn, J. R.; Olson, T.; Pylypenko, S.; Atanassov, P.; Ustinov, E. A. Cross-Laboratory Experimental Study of Non-Noble-Metal Electrocatalysts for the Oxygen Reduction Reaction. *ACS Appl. Mater. Interfaces* **2009**, *1*, 1623−1639.
(8) Fu, X.; Zamani, P.; Choi, J. Y.; Hassan, F. M.; Jiang, G.; Higgins, D. C.; Zhang, Y.; Hoque, M. A.; Chen, Z. In Situ Polymer Graphenization Ingrained with Nanoporosity in a Nitrogenous Electrocatalyst Boosting the Performance of Polymer-Electrolyte-Membrane Fuel Cells. *Adv. Mater.* **2017**, *29*, 1604456−1−1604456−8.
(9) Proietti, E.; Jaouen, F.; Lefevre, M.; Larouche, N.; Tian, J.; Herranz, J.; Dodelet, J. P. Iron-Based Cathode Catalyst with Enhanced Power Density in Polymer Electrolyte Membrane Fuel Cells. *Nat. Commun.* **2011**, *2*, 416−1−416−9.
(10) Wang, Y. C.; Lai, Y. J.; Song, L.; Zhou, Z. Y.; Liu, J. G.; Wang, Q.; Yang, X. D.; Chen, C.; Shi, W.; Zheng, Y. P.; Rauf, M.; Sun, S. G. S-Doping of an Fe/N/C ORR Catalyst for Polymer Electrolyte Membrane Fuel Cells with High Power Density. *Angew. Chem., Int. Ed.* **2015**, *54*, 9907−9910.
(11) Shui, J.; Chen, C.; Grabstanowicz, L.; Zhao, D.; Liu, D. J. Highly Efficient Nonprecious Metal Catalyst Prepared with Metal−Organic Framework in a Continuous Carbon Nanofibrous Network. *Proc. Natl. Acad. Sci. U. S. A.* **2015**, *112*, 10629−10634.
(12) Nabae, Y.; Nagata, S.; Hayakawa, T.; Niwa, H.; Harada, Y.; Oshima, M.; Isoda, A.; Matsunaga, A.; Tanaka, K.; Aoki, T. Pt-Free Carbon-Based Fuel Cell Catalyst Prepared from Spherical Polyimide for Enhanced Oxygen Diffusion. *Sci. Rep.* **2016**, *6*, 23276.
(13) Tong, L.; Shao, Z. G.; Qian, Y. S.; Li, W. M. Facile Ionothermal Synthesis of Mesoporous Fe−N_x−C Composites as Efficient Catalysts for Oxygen Reduction in Acid Media. *J. Mater. Chem. A* **2017**, *5*, 3832−3838.
(14) Zhang, G.; Chenitz, R.; Lefèvre, M.; Sun, S.; Dodelet, J. P. Is Iron Involved in the Lack of Stability of Fe/N/C Electrocatalysts Used to Reduce Oxygen at the Cathode of PEM Fuel Cells? *Nano Energy* **2016**, *29*, 111−125.
(15) Liu, Y.; Ishihara, A.; Mitsushima, S.; Kamiya, N.; Ota, K. Zirconium Oxide for PEFC Cathodes. *Electrochem. Solid-State Lett.* **2005**, *8*, A400−A402.
(16) Kim, J. H.; Ishihara, A.; Mitsushima, S.; Kamiya, N.; Ota, K. Catalytic Activity of Titanium Oxide for Oxygen Reduction Reaction as a Non-Platinum Catalyst for PEFC. *Electrochim. Acta* **2007**, *52*, 2492−2497.
(17) Ishihara, A.; Doi, S.; Mitsushima, S.; Ota, K. Tantalum (oxy)Nitrides Prepared Using Reactive Sputtering for New Non-platinum Cathodes of Polymer Electrolyte Fuel Cell. *Electrochim. Acta* **2008**, *53*, 5442−5450.
(18) Chisaka, M.; Iijima, T.; Yaguchi, T.; Sakurai, Y. Carbon-Supported Hafnium Oxynitride as Cathode Catalyst for Polymer Electrolyte Membrane Fuel Cells. *Electrochim. Acta* **2011**, *56*, 4581−4588.
(19) Chisaka, M. Transition Metal Oxide, Oxynitride, and Nitride Electrocatalysts with and without Supports for Polymer Electrolyte Fuel Cell Cathodes. In *Electrocatalysts for Low Temperature Fuel Cells: Fundamentals and Recent Trends*; Maiyalagan, T., Saji, V. S., Eds.; Wiley-VCH: Weinheim, 2017; pp 423−441.
(20) Liu, G.; Zhang, H.; Wang, M.; Zhong, H.; Chen, J. Preparation, Characterization of ZrO_xN_y/C and its Application in PEMFC as an Electrocatalyst for Oxygen Reduction. *J. Power Sources* **2007**, *172*, 503−510.
(21) Ohnishi, R.; Katayama, M.; Takanabe, K.; Kubota, J.; Domen, K. Niobium-Based Catalysts Prepared by Reactive Radio-Frequency Magnetron Sputtering and Arc Plasma Methods as Non-Noble Metal Cathode Catalysts for Polymer Electrolyte Fuel Cells. *Electrochim. Acta* **2010**, *55*, 5393−5400.
(22) Chisaka, M.; Iijima, T.; Suzuki, Y.; Sakurai, Y. Effect of Synthesis Route on Oxygen Reduction Reaction Activity of Carbon-Supported Hafnium Oxynitride in Acid Media. *J. Phys. Chem. C* **2011**, *115*, 20610−20617.
(23) Seo, J.; Cha, D.; Takanabe, K.; Kubota, J.; Domen, K. Electrodeposited Ultrafine NbO_x, ZrO_x, and TaO_x Nanoparticles on Carbon Black Supports for Oxygen Reduction Electrocatalysts in Acidic Media. *ACS Catal.* **2013**, *3*, 2181−2189.
(24) Ishihara, A.; Chisaka, M.; Ohgi, Y.; Matsuzawa, K.; Mitsushima, S.; Ota, K. Synthesis of Nano-TaO_x Oxygen Reduction Reaction Catalysts on Multi-Walled Carbon Nanotubes Connected via a Decomposition of Oxy-tantalum Phthalocyanine. *Phys. Chem. Chem. Phys.* **2015**, *17*, 7643−7647.
(25) Chisaka, M.; Ishihara, A.; Uehara, N.; Matsumoto, M.; Imai, H.; Ota, K. Nano-TaO_xN_y Particles Synthesized from Oxy-tantalum Phthalocyanine: How to Prepare Precursors to Enhance the Oxygen Reduction Reaction Activity after Ammonia Pyrolysis? *J. Mater. Chem. A* **2015**, *3*, 16414−16418.
(26) Chisaka, M.; Ishihara, A.; Morioka, H.; Nagai, T.; Yin, S.; Ohgi, Y.; Matsuzawa, K.; Mitsushima, S.; Ota, K. Zirconium Oxynitride-Catalyzed Oxygen Reduction Reaction at Polymer Electrolyte Fuel Cell Cathodes. *ACS Omega* **2017**, *2*, 678−684.
(27) Kinumoto, T.; Sou, Y.; Ono, K.; Matsuoka, M.; Arai, Y.; Tsumura, T.; Toyoda, M. Preparation of Fibrous Titania Oxynitride − Carbon Catalyst and Oxygen Reduction Reaction Analysis in Both Acidic and Alkaline Media. *J. Power Sources* **2015**, *273*, 136−141.
(28) Chisaka, M.; Muramoto, H. Reduced Graphene-Oxide-Supported Titanium Oxynitride as Oxygen Reduction Reaction Catalyst in Acid Media. *ChemElectroChem* **2014**, *1*, 544−548.
(29) Sebastián, D.; Baglio, V.; Sun, S.; Tavares, A. C.; Aricò, A. S. Graphene-Supported Substoichiometric Sodium Tantalate as a Methanol-Tolerant, Non-Noble-Metal Catalyst for the Electroreduction of Oxygen. *ChemCatChem* **2015**, *7*, 911−915.
(30) Chisaka, M.; Itagaki, N. Evaluation and Enhancement of the Oxygen Reduction Reaction Activity on Hafnium Oxide Nanoparticles Assisted by L(+)-lysine. *Electrochim. Acta* **2016**, *201*, 279−285.
(31) Reiser, C. A.; Bregoli, L.; Patterson, T. W.; Yi, J. S.; Yang, J. D.; Perry, M. L.; Jarvi, T. D. A. Reverse-Current Decay Mechanism for Fuel Cells. *Electrochem. Solid-State Lett.* **2005**, *8*, A273−A276.
(32) Ioroi, T.; Senoh, H.; Yamazaki, S.; Siroma, Z.; Fujiwara, N.; Yasuda, K. Stability of Corrosion-Resistant Magnéli-Phase Ti_4O_7-Supported PEMFC Catalysts at High Potentials. *J. Electrochem. Soc.* **2008**, *155*, B321−B326.
(33) Huang, S. Y.; Ganesan, P.; Park, S.; Popov, B. N. Development of a Titanium Dioxide-Supported Platinum Catalyst with Ultrahigh Stability for Polymer Electrolyte Membrane Fuel Cell Applications. *J. Am. Chem. Soc.* **2009**, *131*, 13898−13899.
(34) Parrondo, J.; Han, T.; Niangar, E.; Wang, C.; Dale, N.; Adjemian, K.; Ramani, V. Platinum Supported on Titanium−Ruthenium Oxide is a Remarkably Stable Electrocatayst for Hydrogen Fuel Cell Vehicles. *Proc. Natl. Acad. Sci. U. S. A.* **2014**, *111*, 45−50.
(35) Tsai, M. C.; Nguyen, T. T.; Akalework, N. G.; Pan, C. J.; Rick, J.; Liao, Y. F.; Su, W. N.; Hwang, B. J. Interplay between Molybdenum Dopant and Oxygen Vacancies in a TiO_2 Support Enhances the Oxygen Reduction Reaction. *ACS Catal.* **2016**, *6*, 6551−6559.

DOI: 10.1021/acsaem.7b00100
ACS Appl. Energy Mater. 2018, 1, 211−219

(36) Chisaka, M.; Ando, Y.; Yamamoto, Y.; Itagaki, N. A Carbon-Support-Free Titanium Oxynitride Catalyst for Proton Exchange Membrane Fuel Cell Cathodes. *Electrochim. Acta* **2016**, *214*, 165−172.
(37) Stamenković, V.; Schmidt, T. J.; Ross, P. N.; Marković, N. M. Surface Composition Effects in Electrocatalysis: Kinetics of Oxygen Reduction on Well-Defined Pt_3Ni and Pt_3Co Alloy Surfaces. *J. Phys. Chem. B* **2002**, *106*, 11970−11979.
(38) Chisaka, M.; Ando, Y.; Muramoto, H. Facile Combustion Synthesis of Carbon-Supported Titanium Oxynitride to Catalyse Oxygen Reduction Reaction in Acidic Media. *Electrochim. Acta* **2015**, *183*, 100−106.
(39) Chisaka, M.; Ando, Y.; Itagaki, N. Activity and Durability of the Oxygen Reduction Reaction in a Nitrogen-Doped Rutile-Shell on TiN-Core Nanocatalysts Synthesised via Solution-Phase Combustion. *J. Mater. Chem. A* **2016**, *4*, 2501−2508.
(40) Bolokang, A. S.; Phasha, M. J. Formation of Titanium Nitride Produced from Nanocrystalline Titanium Powder under Nitrogen Atmosphere. *Int. J. Refract. Hard Met.* **2010**, *28*, 610−615.
(41) Sato, S.; Nakamura, R.; Abe, S. Visible-Light Sensitization of TiO_2 Photocatalysts by Wet-method N Doping. *Appl. Catal., A* **2005**, *284*, 131−137.
(42) Saha, N. C.; Tompkins, H. G. Titanium Nitride Oxidation Chemistry: An X-ray Photoelectron Spectroscopy Study. *J. Appl. Phys.* **1992**, *72*, 3072−3079.
(43) Robinson, K. S.; Sherwood, P. M. A. X-ray Photoelectron Spectroscopic Studies of the Surface of Sputter Ion Plated Films. *Surf. Interface Anal.* **1984**, *6*, 261−266.
(44) Avasarala, B.; Murray, T.; Li, W.; Haldar, P. Titanium Nitride Nanoparticles Based Electrocatalysts for Proton Exchange Membrane Fuel Cells. *J. Mater. Chem.* **2009**, *19*, 1803−1805.
(45) Wang, J.; Zhu, W.; Zhang, Y.; Liu, S. An Efficient Two-Step Technique for Nitrogen-Doped Titanium Dioxide Synthesizing: Visible-Light-Induced Photodecomposition of Methylene Blue. *J. Phys. Chem. C* **2007**, *111*, 1010−1014.
(46) Yang, G.; Jiang, Z.; Shi, H.; Xiao, T.; Yan, Z. Preparation of Highly Visible-Light Active N-Doped TiO_2 Photocatalyst. *J. Mater. Chem.* **2010**, *20*, 5301−5309.
(47) Shaw, W. H. R.; Bordeaux, J. J. The Decomposition of Urea in Aqueous Media. *J. Am. Chem. Soc.* **1955**, *77*, 4729−4733.
(48) Zhu, R. S.; Wang, J. H.; Lin, M. C. Sublimation of Ammonium Salts: A Mechanism Revealed by a First-Principles Study of the NH_4Cl System. *J. Phys. Chem. C* **2007**, *111*, 13831−13838.
(49) Zakorzhevskii, V. V.; Kovalev, I. D.; Barinov, Y. N. Self-Propagating High-Temperature Synthesis of Titanium Nitride with the Participation of Ammonium Chloride. *Inorg. Mater.* **2017**, *53*, 278−286.

DOI: 10.1021/acsaem.7b00100
ACS Appl. Energy Mater. 2018, 1, 211−219